CGI2013 Geometry Processing Workshop manuscript No.
(will be inserted by the editor)

A Geometrical Framework to Capture the Dynamical Evolution of Slow-Fast Vector Fields

Martin Gutschke, Alexander Vais and Franz-Erich Wolter

Abstract In this work we present computational methods dealing with dynamical systems. We focus on those systems being characterized by slow-fast vector fields or corresponding differential algebraic equations that commonly occur in physical applications. In the latter one usually considers a manifold of admissible physical states and a vector field describing the evolution of the physical system over time. The manifold is embedded within a higher-dimensional space and is implicitly defined by a system of equations. Certain physical systems, such as so-called relaxation oscillators, perform sudden jumps in their state evolution which are difficult to model. The main contribution of the present work is to approach this problem from a geometric perspective which provides not only a qualitative analysis but also produces quantitative results. We describe techniques for explicitly computing parametrizations of the implicitly defined manifold and of the relevant jump and hit sets. This allows us to compute the dynamical evolution of the system including the aforementioned jump phenomena. As main tools we use homotopy approaches in conjunction with tools from differential geometry such as geodesic polar coordinates. We discuss how to numerically realize and how to apply them to several examples from mechanics, electrical engineering and biology.

1 Introduction

Many physical systems can be characterized by their state $w(t)$ that they are currently in for a time parameter t. The set of all states has the structure of a space where nearby points correspond to similar states. Additionally, one encounters constraints that reduce the total state space to a subspace of admissible states. Mathematically this situation is modeled within the setting of differential geometry by considering the space of admissible states to be an m-dimensional regular submanifold M of a larger ambient space $\mathbb{R}^k$. Here m is the number of degrees of freedom for the physical system, while k is chosen sufficiently large in order to capture all relevant parameters of the model under investigation. Moreover, the aforementioned constraints are expressed as equations in the state variables, allowing us to define M implicitly as the zero set of a sufficiently regular function, see e.g. [10]:

$$M := f^{-1}(0) \quad \text{for} \quad f : \mathbb{R}^k \to \mathbb{R}^n,\ n = k - m\ .$$

To model the dynamical behavior of the considered physical system over time, one considers a one-parameter family of mappings $\phi_t : M \to M$, describing how a state w evolves into a state $\phi_t(w)$ after time t has elapsed. A more localized description can be given in terms of a tangential vector field $X_T : M \to TM$ on M describing the infinitesimal changes of the system such that

$$\frac{d}{dt}\phi_t(w) = X_T(\phi_t(w))\ .$$

Such a formulation arises for example in the context of Newtonian mechanics where a state in the state space corresponds to position and velocity information while external forces give rise to a vector field that describes the local dynamic behavior. The global description can be recovered by integrating the above ordinary differential equation, thus computing the trajectory $t \mapsto \phi_t(w)$ of X_T.

The aforementioned constraints are in practice often idealizations of a process inducing a fast evolution towards an admissible state. Vice versa, given a description of the fast evolution in terms of a fast vector field,

Welfenlab, Leibniz University Hannover
{gutschke,vais,few}@welfenlab.de

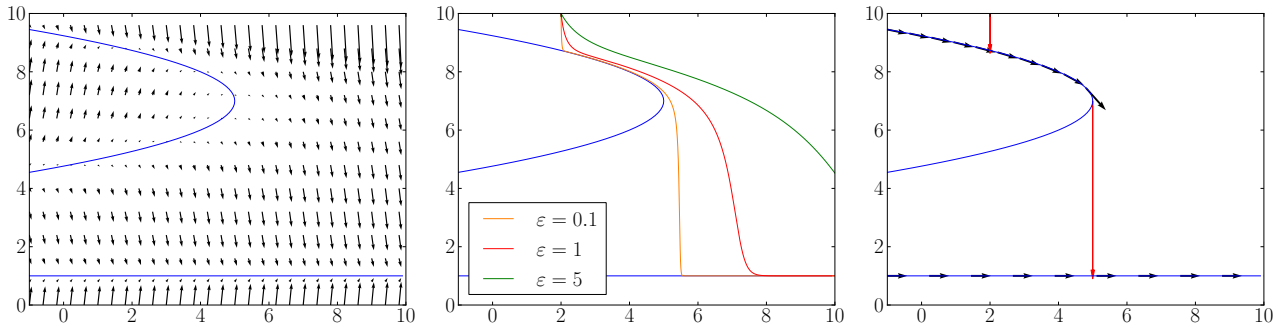

(a) (b) (c)

Fig. 1: Example for a slow-fast vector field.

one can consider its equilibria to define the manifold of admissible states. Thus, the whole dynamical evolution of the non-idealized system can be described in terms of a vector field X on the larger ambient space $\mathbb{R}^k$ which is decomposed into a fast and a slow component, i.e. $X = F + S$. The fast component F dominates, leading to a fast flow towards the state manifold M, where it vanishes. Thus M consists of equilibrium points of F. By looking at the linearization of F in the points of M, one can classify those according to whether they constitute stable or instable equilibria.

As an introductory example let V_ε be the following vector field within in $\mathbb{R}^2$

$$V_\varepsilon(x,y) = \begin{pmatrix} 1 \\ \frac{1}{\varepsilon} f(x,y) \end{pmatrix} = \underbrace{\begin{pmatrix} 0 \\ \frac{1}{\varepsilon} f(x,y) \end{pmatrix}}_{F(x,y)} + \underbrace{\begin{pmatrix} 1 \\ 0 \end{pmatrix}}_{S(x,y)}$$

with $f(x,y) = (x + (7-y)^2 - 5)(y-1)$ and a small ε as depicted in Fig. 1a. It decomposes into a fast part F and a slow part S, where F vanishes on $M = \{f(x,y) = 0\}$.

Consider a fixed initial point $w \in \mathbb{R}^2$. Figure 1b shows its trajectory as determined by V_ε for various ε. Observe, that if w is not contained in a sufficiently small neighbourhood of M then the fast component of V_ε will force the corresponding trajectory to quickly approach M. As ε tends to zero, this happens in an almost instantaneous fashion. In the vicinity of M the trajectory is basically determined by the slow component S of the vector field which leads towards the vertex of the parabola. At the latter point, which can be seen as a kind of fold with respect to the y direction, the dynamical evolution will perform a sudden jump vertically downwards along the fast vector field F until it reaches the lower part of M where it continues as controlled by S.

The phenomena occurring in this example for $\varepsilon \to 0$, most notably the jumps occurring at the fold of the manifold, see Fig. 1c, are characteristic for many physical systems that exhibit fast switching behavior, see e.g. [15]. The points on M where the jumps begin constitute the so-called jump set α. The points on the manifold hit after a jump will constitute the so-called hit set β. Thus the jump itself can be modeled as a map $\pi : \alpha \to \beta$.

By combining the description of the admissible state manifold and the description of the dynamical state evolution in terms of a vector field, one obtains a so-called differential algebraic equation (DAE) system. We will denote it compactly in the form:

$$f(x,y) = 0 \quad \text{and} \quad g(x,y,X) = 0\ , \tag{1}$$

where $f : \mathbb{R}^m \times \mathbb{R}^n \to \mathbb{R}^n$ and $g : \mathbb{R}^m \times \mathbb{R}^n \times \mathbb{R}^k \to \mathbb{R}^k$ are given sufficiently regular functions. Here the first equation describes the state or slow manifold $M \subset \mathbb{R}^k$ while the second one determines a vector field X on the ambient space. In this description the fast vector field is modeled by jumps within the subspace spanned by the y variables. As discussed in e.g. [7] a sufficient condition for a point p to lie on the jump set α is given by

$$\det\left(\frac{\partial f(p)}{\partial y}\right) = 0\ . \tag{2}$$

We will show how this equation can be used to determine the jump set in practice.

While fast switching behavior has been studied from a theoretical perspective by many authors, see e.g. [26, 21, 8, 9, 7, 15] comparatively little research has focused on computational approaches.

A main contribution of the present work is to provide a set of geometrically motivated numerical techniques to deal with slow-fast vector fields or corresponding differential algebraic equations. These methods have been designed to be largely independent of dimension in order to achieve a high degree of flexibility with respect to the classes of examples supported. Our approach can deal with manifolds and vector fields implicitly defined by nonlinear equations by adapting ho-

motopy techniques and numerical continuation methods adequately [25, 3]. Furthermore we use geodesic polar coordinates [4] to obtain an efficient parametrization and intuitively easily comprehensible visualization of all computed objects.

A key point in our method is the pre-calculation of the jump and hit sets, thereby enabling an explicit calculation of the jumps induced by the fast vector field. This provides an efficient and numerically stable alternative to traditional methods which are confined to tracing the slow-fast vector field without making use of the slow manifold. Our geometrically inspired approach has been successfully applied in the context of electrical engineering where it improves the stability of circuit simulators by dispensing with the so-called Tikhonov regularization, see [11, 17, 19]. Besides electrical engineering, our approach is quite flexible and therefore able to deal with a variety of examples inspired by physical applications.

2 Basics and notation

Consider a manifold M embedded in $\mathbb{R}^k$ and implicitly defined by $f(w) = 0$ where $f : \mathbb{R}^k \to \mathbb{R}^n$. Here $k = n + m$ where m is the dimension of M while n is the so-called co-dimension. We will denote by $f^i : \mathbb{R}^k \to \mathbb{R}$ the component functions of f. Also we will decompose $w \in \mathbb{R}^k$ according to $w = (x, y)$ with $x \in \mathbb{R}^m$ and $y \in \mathbb{R}^n$ being referred to as the slow and fast variables, respectively.

In this paper we will denote the Jacobian matrix of f in a point p by J, or in components by $J_{ij} = \frac{\partial f^i(p)}{\partial w^j}$. The tangent space T_pM of M in p is given by the kernel of J, i.e $T_pM = \{v \in T_p\mathbb{R}^k : Jv = 0\}$. The orthogonal complement of T_pM within $T_p\mathbb{R}^k$ is the so-called normal space which we will denote by N_pM and is spanned by the columns ∇f^i of J^T. The dimension of T_pM is obviously m while the dimension of N_pM equals the co-dimension n. As a basis of $T_p\mathbb{R}^k$ we choose the canonical basis $e_1, \ldots, e_k$. A basis of T_pM will be denoted by $b_1, \ldots, b_m$.

The Jacobian can be used to project any vector $X \in T_p\mathbb{R}^k$ into T_pM, see Fig. 2. For the so-called orthogonal projection we write

$$X = X_T + X_N = X_T + \sum_{i=1}^{n} \nabla f^i u^i = X_T + J^T u \qquad (3)$$

with $u \in \mathbb{R}^n$. Here $X_T \in T_pM$ while $X_N = J^T u \in N_pM$. Multiplying from the left with J leads to

$$JX = JX_T + JJ^T u = JJ^T u \implies u = (JJ^T)^{-1} JX \ .$$

By solving for u and back-substitution we obtain

$$X_T = X - J^T u = X - J^T (JJ^T)^{-1} JX \ .$$

The expression $J^T(JJ^T)^{-1}$ is the so-called Moore-Penrose pseudo-inverse of J in case J is of full rank and has more columns than rows. It can be computed efficiently using standard methods such as the singular value decomposition, see[6]. We will denote it in short by J^+. Thus we can write the orthogonal projection as

$$X_T = X - J^+ JX \ . \qquad (4)$$

Aside from the orthogonal projection we will also need a parallel projection along the subspace spanned by the n vectors $e_{m+1}, \ldots, e_k$. We collect those vectors as column vectors forming a matrix $Y \in \mathbb{R}^{k \times n}$. Analogous to equation (3) we write $X = X_T + Yu$ for some $u \in \mathbb{R}^n$. Multiplying by J yields

$$JX = JX_T + JYu = JYu \quad \implies \quad u = (JY)^{-1} JX \ .$$

Note that $JY = \frac{\partial f}{\partial y}$ is has full rank for points not lying on the jump set. Thus we obtain

$$X_T = X - Y(JY)^{-1} JX \ . \qquad (5)$$

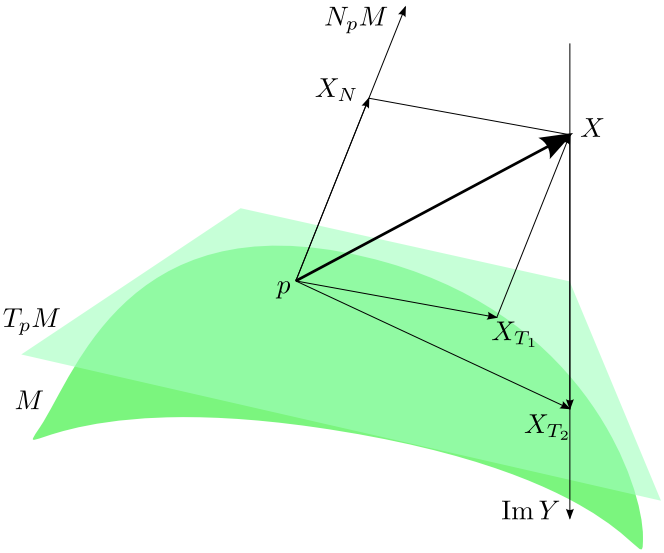

Fig. 2: Two ways of projecting a vector $X \in \mathbb{R}^k$ into the tangent space T_pM. Orthogonal projection yields X_{T_1} while X_{T_2} results from a parallel projection along the direction given by $\operatorname{Im} Y$.

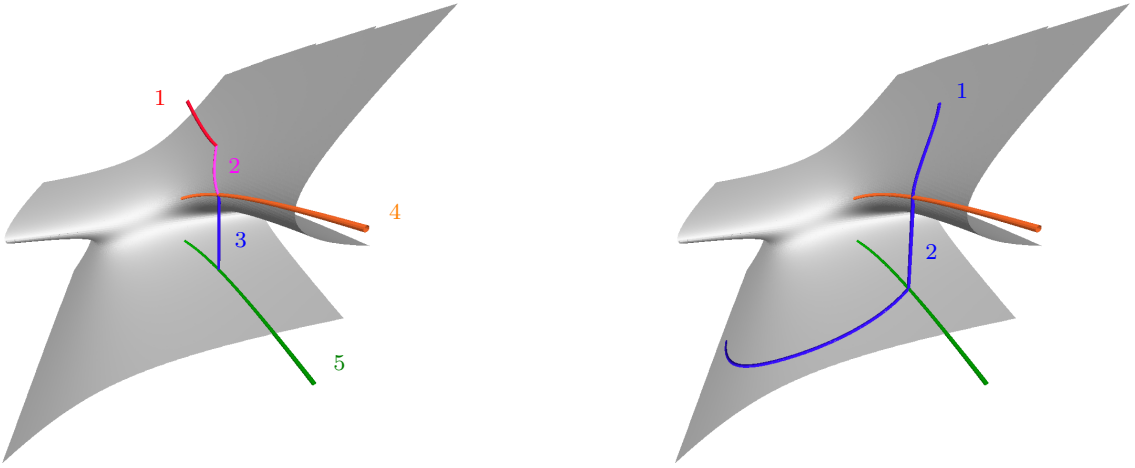

(a) Preprocessing phase: 1.) Determine an initial point on M. 2.) Find the jump set using geodesics. 3.) Calculate a corresponding initial point on the hit set. 4,5.) Determine jump and hit set.

(b) Tracing phase: Starting from a point on M compute the trajectory of the slow vector field incorporating jumps, see 1 and 2 respectively.

Fig. 3: Overview of the steps of our approach.

3 Our approach

Starting with a DAE system as given by equation (1), our approach can be split into three phases: preprocessing, tracing and visualization.

The **preprocessing phase** is used to locate and parametrize the jump and hit set on the state manifold M. It consists of the following steps:

- Find an initial point w_* on M, see Sec. 3.1.
- Starting from w_* use geodesics to find an initial point α_0 on the jump set as discussed in Sec. 3.2.
- Determine the point β_0 on the hit set corresponding to α_0 c.f. Sec. 3.3 and trace the jump set α and the hit set β simultaneously, thereby obtaining the jump map $\pi : \alpha \to \beta$. This is discussed in Sec. 3.4 and Sec. 3.5 for one and two-dimensional jump sets, respectively.

In the **tracing phase** we are given an initial point η_0 on M, possibly in terms of geodesic polar coordinates with respect to w_*. Using the data collected above allows us to compute the trajectory of the slow dynamic passing through η_0 and to approximate the fast dynamic by jumps as discussed in Sec. 3.6. The preprocessing and tracing phases of our approach are graphically summarized in Fig. 3.

Finally, in the **visualization phase**, the parametrization of the resulting trajectory can be visualized and analyzed in various ways to extract useful information. In Sec. 3.7 we will discuss the use of geodesic polar coordinates to visualize our results for two-dimensional manifolds. A discussion of several computational examples is given in Sec. 4.

3.1 Homotopy methods for finding starting-points

In order to perform computations on an implicitly defined manifold M it has to be localized within the larger ambient space $\mathbb{R}^k$. In principle this amounts to finding all solutions w satisfying $f(w) = 0$. As the function f is nonlinear in general, it is not obvious how to solve this system of equations to obtain a parametrization of the solution set. Especially for high co-dimension it can be difficult to locate even a single point of M. As a first step, our approach consists of finding a single solution w_* by a homotopy method described below. This solution will be used as a starting point for the subsequent computations, especially for introducing geodesic polar coordinates on M.

In order to find a starting point, we set up a homotopy between the nonlinear system $f(w) = 0$ and a simpler equation such as $f(w) - f(w_0) = 0$. The latter equation can be solved trivially given an arbitrary point w_0 in the ambient space which does not necessarily have to satisfy $f(w_0) = 0$. A suitable homotopy can be formulated by linearly interpolating between the two equations using a parameter $\lambda \in [0, 1]$:

$$H(w, \lambda, w_0) = f(w) + (\lambda - 1)f(w_0) \ . \tag{6}$$

This is similar to the so-called Newton homotopy which is discussed for example in [3]. An alternative based on the so-called fixed-point homotopy is defined as

$$H(w, \lambda, w_0) = \lambda f(w) + (1 - \lambda)(w - w_0) \ .$$

For a fixed w_0, the zero set of the function H is in general a $(k+1-n)$-dimensional submanifold of $\mathbb{R}^k \times \mathbb{R}$.

We will call a curve in this submanifold a zero curve of the homotopy function and parametrize it as $w = w(t)$ and $\lambda = \lambda(t)$ using a free parameter t. Substituting these expressions into the homotopy function we obtain the following equation for the zero curve:

$$H(w(t), \lambda(t), w_0) = 0 \ . \tag{7}$$

By construction we have for $\lambda = 0$:

$$H(w_0, 0, w_0) = 0$$

while for $\lambda = 1$ we obtain

$$H(w_*, 1, w_0) = f(w_*) = 0 \ .$$

Therefore, assuming that $(w_0, 0)$ and $(w_*, 1)$ lie on the same connected component of the zero curve, we can reach the point $(w_*, 1)$ by tracing the path connecting these two points, finally yielding the desired starting point w_*. Assuming H to be given by eq. (6) we differentiate eq. (7) to yield

$$J(w)\dot{w}(t) + f(w_0)\dot{\lambda}(t) = 0 \ .$$

Note that this equation is a linear system for the vector $(\dot{w}, \dot{\lambda})$. It consists of n equations for $k+1$ unknowns. Therefore, assuming J has full rank, this system has a $(k+1-n)$-dimensional solution space. We choose $(\dot{w}, \dot{\lambda})$ to be a vector with smallest L_2 norm within this space. An additional choice of orientation defines a unique tangent vector $(\dot{w}, \dot{\lambda})$ that can be used to trace the zero curve employing standard ODE solvers or predictor-corrector methods. For many purposes it suffices to assume that the zero curve can be parametrized monotonously by λ and therefore we can set $\dot{\lambda} = 1$. In this case we obtain the initial value problem

$$\dot{w} = -J^+ f(w_0) = -J^+ f(w_0) \ , \quad w_0 = w(0) \ . \tag{8}$$

This method can fail due to an unsuitable choice of w_0 if the zero curve containing w_0 does not reach $\lambda = 1$. Tracing might also stop in case a singularity occurs. Therefore the homotopy approach does not guarantee to yield a solution. However, as suggested by the theorem of Sard, these problems can often be easily avoided by applying a small shift to w_0 and restarting the algorithm with the new homotopy function. See also the discussion in [3] for more details on these issues.

Note that the described method can be regarded as an extension of classical homotopy approaches which are designed to handle the computation of isolated zeros of a function $f : \mathbb{R}^k \to \mathbb{R}^k$. In our case, the dimension of the co-domain of f is n which is smaller than k. Therefore there are many possible zero curves. We pick out a particular curve by choosing its tangent vector according to equation (8).

We encountered no difficulties in all of our computational examples using the above strategy. We have tested our method on several geometrically motivated examples and also on some physical examples provided by nonlinear electric circuits [18], [19] which are numerically less well-behaved. This suggests that the extended homotopy approach is a useful tool for finding points on implicitly defined manifolds in practice.

3.2 Tracing geodesics on an implicit submanifold

Our later computations benefit from a parametrization of the manifold M. Since the co-dimension is possibly high and due to the folded nature of our manifold, this is in general a difficult task. In this setting it is advantageous to introduce geodesic polar coordinates (GPCs) [4]. These are a generalization of the well-known Euclidean polar coordinates which describe the location of a point $q \in \mathbb{R}^m$ by its distance s along a ray through p emanating from the origin, while the direction of the ray is specified by $m-1$ angular parameters $\varphi_1, \ldots, \varphi_{m-1}$. For the GPCs the origin is replaced by some point γ_0 in M while the rays are replaced by so-called geodesics on M that emanate from γ_0.

The theorem of Hopf-Rinow [4] implies that on any finite-dimensional, complete and connected Riemannian manifold a given pair of points can be joined by a geodesic. In our context it implies especially that we can cover M by geodesic polar coordinates. An example illustrating those is shown in Fig. 4, where several geodesics emanating from a central point and some corresponding geodesic circles are depicted. Restricting the length of every geodesic in a GPC system such that it is the shortest path joining its end points, the GPC essentially provide a bijective parametrization of M. Here

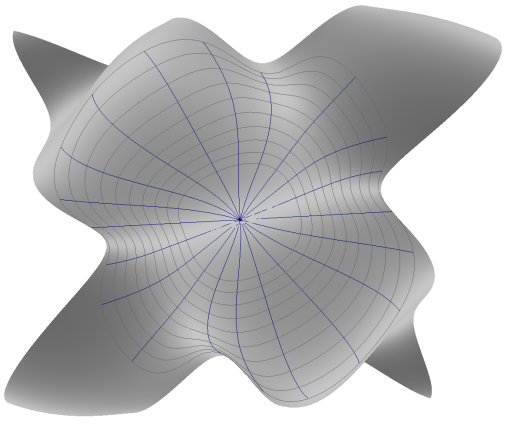

Fig. 4: Isolines of geodesic polar coordinates.

the injectivity of the GPC is violated only on the cut locus of γ_0, see [22].

A geodesic emanating from γ_0 is a locally shortest curve $\gamma : [0, \infty) \to M$ with $\gamma(0) = \gamma_0$, whose initial tangent direction $\dot{\gamma}(0)$ is given by a unit vector in $T_{\gamma_0}M$. It is well-known that geodesics are also the locally straightest curves in M, meaning that their geodesic curvature in M vanishes, see e.g. [4]. Moreover, their straightness is characterized by the so-called geodesic differential equations that we will now derive in our setting, where M is defined implicitly by the equation $f(w) = 0$. For an alternative treatment we refer to [5] .

First of all, the geodesic $\gamma : [0, \infty) \to \mathbb{R}^k$ is a curve located on the manifold, therefore it must satisfy the equation $f^l(\gamma(t)) = 0$ for all $l = 1, \ldots, n$. By differentiating this equation with respect to t we obtain

$$\sum_{i=1}^{k} \frac{\partial f^l}{\partial w^i} \dot{\gamma}^i = 0 \ ,$$

while differentiating again yields

$$\sum_{i,j=1}^{k} \frac{\partial^2 f^l}{\partial w^i \partial w^j} \dot{\gamma}^i \dot{\gamma}^j + \sum_{i=1}^{k} \frac{\partial f^l}{\partial w^i} \ddot{\gamma}^i = 0 \ . \tag{9}$$

Since the geodesic γ is a locally straightest curve, which we assume to be parametrized by arc-length, the tangential component of $\ddot{\gamma}(t)$ vanishes, c.f. [4]. Thus according to eq. (4) we have $J^+ J \ddot{\gamma} = \ddot{\gamma}$. Multiplying the above equation by J^+_{rl} and summing over l we obtain

$$\ddot{\gamma}^r = -\sum_{l=1}^{n} \sum_{i,j=1}^{k} J^+_{rl} \frac{\partial^2 f^l}{\partial w^i \partial w^j} \dot{\gamma}^i \dot{\gamma}^j \ .$$

In order to numerically integrate these equations we need initial values for $\gamma(0)$ and $\dot{\gamma}(0)$. The former are provided by $\gamma^l(0) = \gamma^l_0$ for $l = 1, \ldots, k$. In order to determine the latter, we use an orthonormal basis (b_i) of $T_{\gamma_0}M$ to construct a unit length vector from the given angular parameters. Note that the basis (b_i) is easily obtained by computing a singular value decomposition of J or employing Gram-Schmidt orthogonalization.

3.3 Initial point of the jump and hit set

Based on the criterion (2) we use a shooting method to find an initial point of the jump set. More precisely, from the point γ_0 on the manifold we shoot geodesics $\gamma(t)$ until the sign of $\det\left(\frac{\partial f(\gamma(t))}{\partial y}\right)$ switches. According to the theorem of Hopf-Rinow [4] this procedure has to succeed if one considers sufficiently long geodesics.

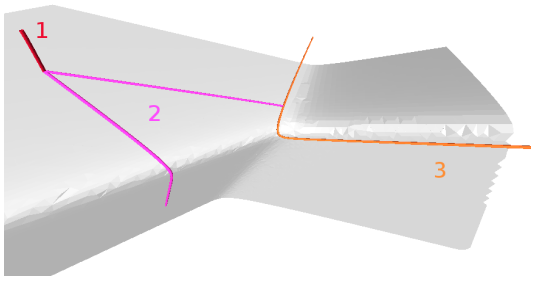

Fig. 5: Illustration of the method used to find the jump set. 1.) Find an initial point on the manifold. 2.) Shoot geodesics in order to find the jump set, marked as 3. Only two geodesics are depicted here.

After finishing this procedure we have two types of coordinates of a point α_0 of the jump set, namely its Cartesian coordinates in ambient space as well as its geodesic polar coordinates on the implicitly defined manifold. Figure 5 illustrates the described method.

Using the matrix Y introduced in Sec. 2, the starting point α_0 of the jump set in combination with the jump space $\operatorname{Im} Y$ can be used to determine a corresponding jump to a point β_0 of the hit set β. More precisely the set $\alpha_0 + \operatorname{Im} Y$ defines an n-dimensional affine subspace containing α_0. Intersecting this subspace with the manifold M provides β_0.

In order to formulate this intersection in terms of equations, write $\alpha_0 = (x_0, y_0)$ where $x_0 \in \mathbb{R}^m$ and $y_0 \in \mathbb{R}^n$. We are interested in determining

$$y_1 \neq y_0 \in \mathbb{R}^n \text{ such that } f(x_0, y_1) = 0 \ ,$$

explicitly illuminating the jump in the fast y variables while the x variables stay constant. The latter condition is a nonlinear system of n equations for the n unknowns in y_1. Solving this system using a homotopy approach yields the point $\beta_0 := (x_0, y_1)$ on the hit set. Note that one needs to exclude the trivial solution $y_1 = y_0$.

3.4 One-dimensional jump and hit sets

Starting from a point α_0 on the jump set our goal is to obtain a parametrization of the jump set α. In this section we assume M to be two-dimensional implicating the jump set to be one-dimensional. The latter can therefore be parametrized by a map $\alpha : \mathbb{R} \to M$. By abuse of notation we will use α to denote the jump set as a set or its parametrization depending on the context.

Since $\alpha \subset M$ and points on α satisfy the determinant criterion characterizing the jump set, we have the

two conditions

$$f(\alpha(t)) = 0 \quad \text{and} \quad \det\left(\frac{\partial f(\alpha(t))}{\partial y}\right) = 0 \ ,$$

which are sufficient to determine α using a numerical continuation method as follows.

We differentiate the above equations with respect to t. While the first equation yields $J\dot{\alpha} = 0$, computing derivatives of the determinant expression is more involved. The determinant is expressed as

$$\det\left(\frac{\partial f(\alpha(t))}{\partial y}\right) = \sum_{\pi} \operatorname{sgn}(\pi) \prod_{r=1}^{n} \frac{\partial f^r}{\partial y^{\pi(r)}} \ ,$$

where the sum extends over all n-permutations. Differentiating the last expression with respect to t yields

$$\sum_{\pi} \operatorname{sgn}(\pi) \sum_{s=1}^{n} \frac{d}{dt}\left(\frac{\partial f^s}{\partial y^{\pi(s)}}\right) \prod_{\substack{r=1 \\ r\neq s}}^{n} \frac{\partial f^r}{\partial y^{\pi(r)}} \ .$$

Finally using the chain rule to express $\frac{d}{dt}(\cdots)$ we can write the derivative of the determinant criterion as

$$\sum_{j=1}^{k} \left(\sum_{\pi} \operatorname{sgn}(\pi) \sum_{s=1}^{n} \frac{\partial^2 f^s}{\partial w^j \partial y^{\pi(s)}} \prod_{\substack{r=1 \\ r\neq s}}^{n} \frac{\partial f^r}{\partial y^{\pi(r)}} \right) \dot{\alpha}^j = 0 \ .$$

Note that the last equation is a linear condition for $\dot{\alpha}$. Together with $J\dot{\alpha} = 0$ this determines a one-dimensional subspace containing $\dot{\alpha}$, which is used within classical ODE solvers or predictor-corrector methods. The only degrees of freedom left are the length of $\dot{\alpha}$ and its sign. In order to parametrize the jump set by arc length one can enforce the condition $\|\dot{\alpha}\| = 1$. The sign ambiguity allows us to choose the tracing direction.

Analogously to the jump set, the hit set can be parametrized as $\beta : \mathbb{R} \to M$. From Sec. 3.3 we already know an initial point β_0 with $\beta(0) = \beta_0$. It is advantageous to compute α and β simultaneously within a numerical continuation method, with the necessary tangent direction $\dot{\beta}$ being obtained as follows. Denoting the jump map by $\pi(x, y) = (x, \pi^y(x, y))$, we fix the parametrization of β by $\beta(t) = \pi(\alpha(t))$. Since $\beta(t)$ lies on the manifold, we have

$$f(\alpha^x(t), \pi^y(\alpha(t))) = 0 \ ,$$

where we have denoted by α^x and α^y the slow and fast components of α. By differentiating with respect to t we obtain

$$\frac{\partial f}{\partial x}\dot{\alpha}^x + \frac{\partial f}{\partial y} d\pi^y \dot{\alpha} = 0 \quad \Rightarrow \quad d\pi^y \dot{\alpha} = -\left(\frac{\partial f}{\partial y}\right)^{-1} \frac{\partial f}{\partial x}\dot{\alpha}^x \ .$$

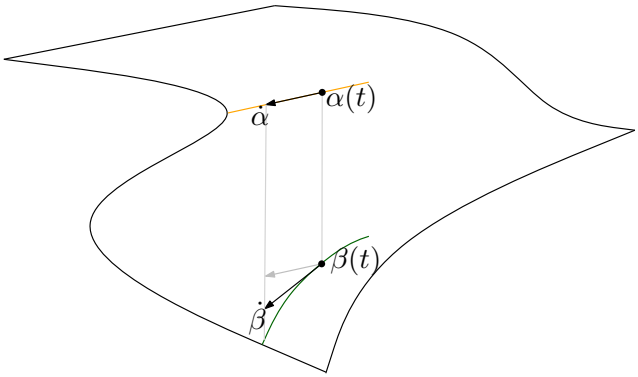

Fig. 6: Computing tangent information for the hit set.

Thus $\dot{\beta}$ is given as

$$\dot{\beta} = d\pi\ \dot{\alpha} = \left(\frac{\mathrm{id}_{\mathbb{R}^m} \mid 0}{d\pi^y}\right)\begin{pmatrix}\dot{\alpha}^x \\ \dot{\alpha}^y\end{pmatrix} = \begin{pmatrix}\dot{\alpha}^x \\ -\left(\frac{\partial f}{\partial y}\right)^{-1}\frac{\partial f}{\partial x}\dot{\alpha}^x\end{pmatrix} \ .$$

As indicated in Fig. 6, the last equation can be geometrically interpreted as applying the projection in eq. (5) to the vector $\dot{\alpha}(t)$, where the latter is considered as lying in $T_{\beta(t)}\mathbb{R}^k$, i.e.

$$\dot{\beta}(t) = \dot{\alpha}(t) - Y(JY)^{-1}J\dot{\alpha}(t) \ , \tag{10}$$

with the Jacobian J of f being evaluated at $\beta(t)$.

Note that the parametrized one-dimensional jump and hit sets can be represented compactly by B-splines for further processing, see e.g. [24, 13].

3.5 Multi-dimensional jump and hit sets

In case the dimension m of the manifold is higher than two, the jump set becomes more than one-dimensional. A parametrization has to be described in terms of a map $\alpha : \mathbb{R}^{m-1} \to M$. The considerations of the previous section still apply to constructing an individual one-dimensional curve lying within the jump set. However, the corresponding equations are not sufficient to determine the tangent direction of the curve uniquely.

In order to overcome this difficulty, we can use geodesic polar coordinates to obtain a parametrization of the jump set. More precisely, let us introduce the function $\widehat{f} : \mathbb{R}^k \to \mathbb{R}^{n+1}$ given by

$$\widehat{f}(w) = \left(f(w), \det\left(\frac{\partial f(w)}{\partial y}\right)\right) \ .$$

The equation $\widehat{f}(w) = 0$ defines the jump set implicitly as an $(m-1)$-dimensional submanifold of $M \subset \mathbb{R}^k$. Within this submanifold we can compute geodesics as described in Sec. 3.2 by using $\widehat{f}$ instead of f.

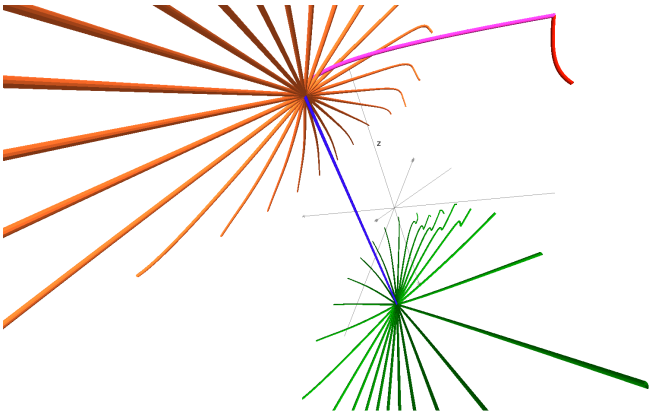

Fig. 7: A two-dimensional jump set, shown in orange, captured by computing geodesics radially emanating from an initial point α_0. The corresponding curves on the hit set emanating from β_0 are shown in green.

Fig. 7 illustrates the method for a two-dimensional jump set. Several geodesics that emanate from an initial point α_0 have been computed, thus inducing geodesic polar coordinates. As discussed in Sec. 3.4, the hit set is parametrized simultaneously by tracing the corresponding projections of those geodesics using eq. (10). Note that this approach includes the one discussed in the previous section as a special case.

3.6 Tracing a vector field on the slow manifold

Assume a vector field $X : M \to \mathbb{R}^k$ to be defined implicitly by

$$g(w, X) = 0 \quad \text{where} \quad g : \mathbb{R}^k \times \mathbb{R}^k \to \mathbb{R}^k \ .$$

At any point $w \in M$ we can project X onto $T_w M$ to yield a vector field $X_T : M \to TM$ on M, which is accomplished using equation (5).

We will assume that X_T is a description of the slow vector field on M. Starting from a given point η_0 on the slow manifold M, our goal is to construct the trajectory $\eta : \mathbb{R} \to M$ of X_T with $\eta(0) = \eta_0$. Denote by $X(t) \in \mathbb{R}^k$ the values of the vector field X described above along η. Thus we have

$$f(\eta(t)) = 0 \ , \quad g(\eta(t), X(t)) = 0 \ .$$

The functions η and X can be computed in parallel by numerically integrating the following system of ordinary differential equations

$$\dot{\eta} = X - Y(JY)^{-1} JX$$
$$\dot{X} = -\left(\frac{\partial g}{\partial X}\right)^{-1} \frac{\partial g}{\partial w} \dot{\eta} \ .$$

Note that the equation for $\dot{\eta}$ describes η as a trajectory of the slow vector field X_T while the equation for $\dot{X}$ follows from differentiating $g(\eta(t), X(t)) = 0$ with respect to t and solving for $\dot{X}$.

Initial conditions are provided by the given point $\eta(0) = \eta_0$ and $X(0) = X_0$. In order to determine X_0 one has to solve the nonlinear system $g(\eta_0, X_0) = 0$ for X_0. The latter step can be done using a suitable homotopy approach. We omit the details here.

3.7 Visualizing objects on M using GPCs

Since curves, such as the jump set, the hit or the slow parts of the computed trajectories lie within the potentially high-dimensional ambient space $\mathbb{R}^k$, it is in general difficult to visualize and understand their shapes and their relative position in terms of a low-dimensional projection. As those curves lie within the m-dimensional manifold $M \subset \mathbb{R}^k$ where $m < k$ it is advantageous to visualize them via an m-dimensional parametrization of M. Since M is defined implicitly, and due to its folded nature, such a parametrization is not readily available. However, geodesic polar coordinates naturally suggest themselves to be used within this context. Due to the dimensionality reduction, visualizing objects on M using polar coordinates allows for a better comprehension of the geometrical relationships. If the manifold is two-dimensional one can intuitively picture this approach as a means to straighten the manifold and the objects on it onto a plane.

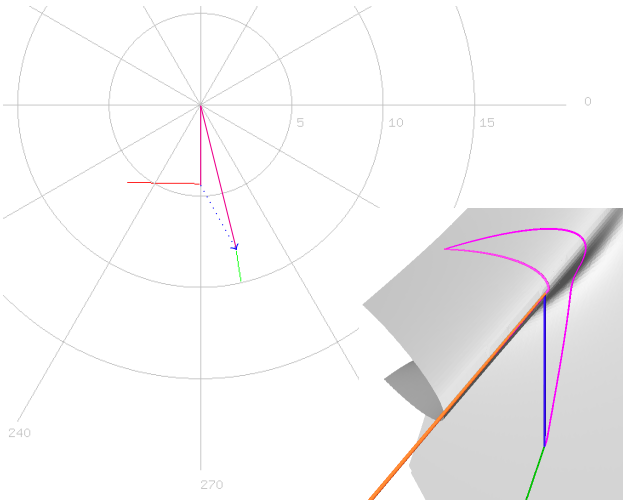

Fig. 8: Visualization via geodesic polar coordinates. The jump set and corresponding hit set are shown in orange resp. green. Additionally two geodesics are drawn in pink. The blue dotted arrow indicates the correspondence between two points related by a jump.

Given a curve α on M, computing its polar coordinates with respect to a point $p \in M$ amounts to the following problem. Let $\gamma : \mathbb{R} \times S^{m-1} \to M$ be the map that sends the polar coordinates (s, φ) to the point $\gamma(s, \varphi)$ in M. The latter is computed by calculating a geodesic curve of length s emanating from p in direction φ and taking its endpoint as discussed in Sec. 3.2. We are now interested in finding the preimages of all points $\alpha(t)$ under γ, thereby solving the equation

$$\gamma(s(t), \varphi(t)) = \alpha(t)$$

for the unknown functions $(s, \varphi) : \mathbb{R} \to \mathbb{R} \times S^{m-1}$. Differentiating the last equation with respect to t one obtains

$$\frac{\partial \gamma}{\partial s}\dot{s} + \frac{\partial \gamma}{\partial \varphi}\dot{\varphi} = \dot{\alpha} \ .$$

This system of linear equations can be solved for $(\dot{s}, \dot{\varphi})$ since $\dot{\alpha}$ is tangential to M provided that $\frac{\partial \gamma}{\partial \varphi}$ has full rank. Thus one can compute $s(t), \varphi(t)$ using classical numerical continuation methods, assuming that the coordinates of an initial point are known. Note that this is the case for the jump set which is found using geodesics as described in Sec. 3.3. Otherwise one can adapt the homotopy approach described in [12].

Note that problems can arise if $\frac{\partial \gamma}{\partial \varphi}$ becomes rank deficient during the numerical continuation, indicating the presence of points which are said to be conjugate to p [4]. In this case, it is beneficial to allow for a reparametrization of α by introducing a free parameter λ, i.e. setting $t = t(\lambda)$ as discussed in [16].

Figure 8 shows an example, visualizing the jump and hit set on a two-dimensional manifold using geodesic polar coordinates.

4 Examples

Our approach has been implemented into a generic and flexible software platform written in C++ in order to apply the proposed methods. For some of our numerical computations we relied upon the Gnu Scientific Library (GSL) while our visualization of the high-dimensional results has been implemented in OpenGL. In order to promote the reproducibility of the results, also a scripting language has been incorporated into the framework.

In order to outline the scope of our methods we will now briefly discuss several examples taken from different scientific fields, illuminating that the approach adopted in this work is flexible enough to deliver numerical results in a variety of practical settings. Although the given examples are only qualitatively discussed, they are taken from applied contexts, incorporating the corresponding physical parameters, such as material constants etc. In particular, the images are designed to give a qualitative impression of the underlying accurately calculated quantitative results.

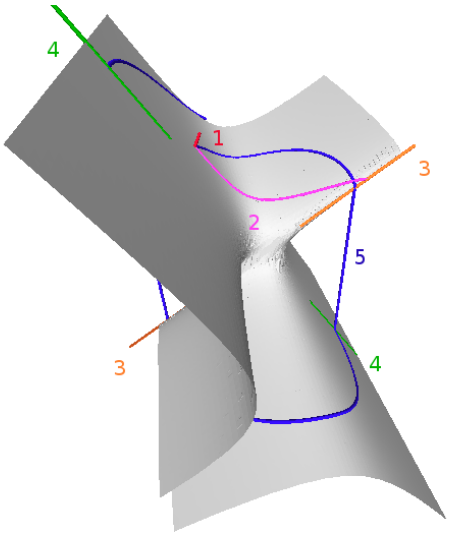

Fig. 9: Artificial 4D example. 1.) Homotopy path leading to an initial point p on M. 2.) Geodesic used to find an initial point on the jump set. 3.) Jump set. 4.) Corresponding hit set. 5.) Trajectory of the slow vector field on M starting from p incorporating two jumps.

The depicted state manifolds are only included for a better understanding as commonly sketched in classical related literature, such as [21]. However they are not necessary within our computational approach.

4.1 Artificial DAE system

As a first example for illustrating our approach, we consider the artificial DAE system given by

$$0 = z^3 - yz^2 + x$$
$$\dot{x} = y$$
$$\dot{y} = -x$$

Here the first equation describes the two-dimensional slow manifold embedded in a three-dimensional space while the other two equations describe a slow vector field curling around the z axis. It is assumed that the fast vector field points along the z axis, thus inducing jumps in z direction. Performing the computations described in the previous sections we obtain the results depicted in Figure 3.

By introducing an additional parameter w we lift the above system to create a second example in which the co-dimension of the slow manifold M is increased from one to two. Thus M is still two-dimensional while

being embedded in a four-dimensional space. The considered equations are

$$
\begin{aligned}
0 &= z^3 - yz^2 - \frac{1}{2}w + \frac{\sqrt{3}}{2}x \\
0 &= \frac{\sqrt{3}}{2}w + \frac{1}{2}x \\
\dot{x} &= -y \\
\dot{y} &= x
\end{aligned}
$$

We assume the jump space to be spanned by the w and z axes. Figure 9 illustrates the individual steps of our approach in this case, showing a three-dimensional projection of the four-dimensional situation.

4.2 Heartbeat

In [26] Zeeman discusses how catastrophe theory can be used in the context of modeling the beating of the heart. In this model, the heartbeat depends on a tension parameter a and a chemical control parameter b. These two parameters span the so-called control plane, and determine the length of the muscle fiber, denoted by x. The dynamical behavior is expressed in terms of a slow-fast vector field in the (a, b, x) space as

$$
\begin{aligned}
\epsilon\dot{x} &= -(x^3 + ax + b) \\
\dot{b} &= x - x_a \\
\dot{a} &= 0
\end{aligned}
$$

Here x_a denotes the diastole length of the fiber. Letting $\epsilon \to 0$ yields the equation of the slow manifold as

$$x^3 + ax + b = 0 \ .$$

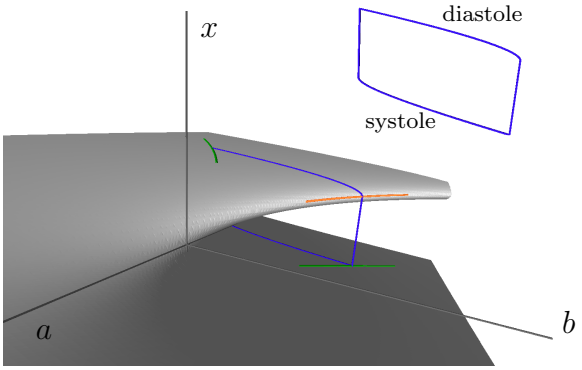

Fig. 10: Results of computations performed using our approach based on equations presented in [26] for describing the beating of the heart. The jump and hit set are shown in orange and green respectively. The closed trajectory represents one cycle of the heartbeat.

Note that the output value x is needed to calculate $\dot{b}$, so the vector field can not be expressed solely in terms of the control parameters.

Figure 10 shows the resulting manifold M, the jump and hit set as well as a trajectory starting from an initial point on M, computed using our approach. Note that a part of the jump set is hidden behind the fold of M and thus not visible from the chosen point of view. The trajectory consists of four parts. Two of those lie on M and are determined by the slow vector field while the other two are jumps approximating the fast vector field. The trajectory is closed, thereby representing one full cycle, i.e. systole and diastole, of the heartbeat.

4.3 Local Nerve Impulse

Another example discussed in [26] is concerned with modeling nerve impulses in axons. It is based on experiments performed by Hodgkin and Huxley in the 1950s, see [2, 1]. An extended discussion of this model can also be found in [14]. Without going into details, the system can be formulated mathematically in terms of the following slow-fast vector field

$$
\begin{aligned}
\dot{x} &= -\frac{1}{\varepsilon}(x^3 + ax + b) \\
\dot{a} &= (x + 0.06(a + 0.5))(x - 1.5a - 1.67) \\
&\quad\ (0.054(b - 0.8)^2 + 0.75) \\
\dot{b} &= -g_K(b + 1.4) - g_{Na}(b - 4.95) - 0.15(b - 0.15)
\end{aligned}
$$

where the values of g_K, g_{Na} depend on a and x and are given by

$$g_K = 2.38 \max(a+0.5, 0) \ , \quad g_{Na} = 16 \min(x+0.5, 0)^2 \ .$$

As before the slow manifold M is obtained by letting $\varepsilon \to 0$ yielding $x^3 + ax + b = 0$.

Consider Figure 11 showing M with the jump and hit sets computed using our approach. From any point on M the slow dynamic given above leads to the equilibrium point E which represents a kind of resting state of the nerve. The application of external influences to the physical system can be modeled by changing the slow vector field. For example, referring to the "voltage clamp experiment" described in [26] applying an external voltage to the nerve displaces the system from E to the point F, thus leaving the manifold. While retaining the constraint $b = const.$, the dynamic of the system leads to the point H. Note that in this example, the vector field is effectively modified by setting $\dot{b} = 0$. The point H is an equilibrium of the modified vector field. By switching off the external voltage, the

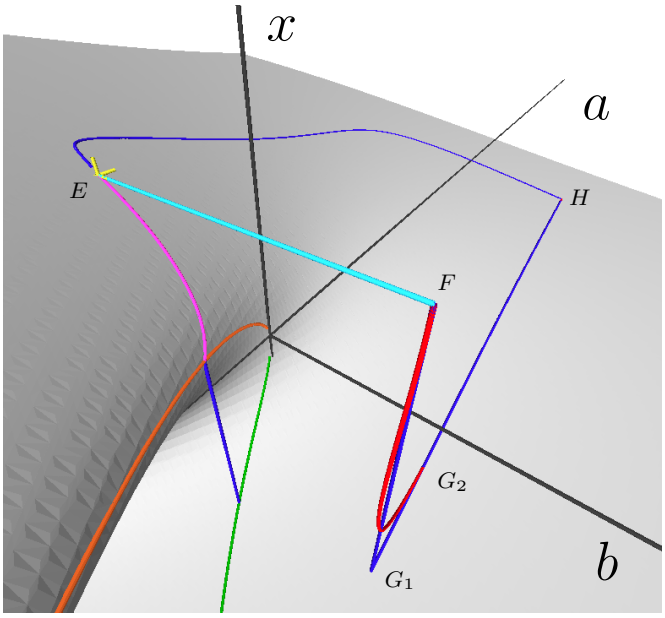

Fig. 11: Results of modeling the nerve impulse along an axon, obtained using our approach. The underlying model is based on [2, 1, 26, 14].

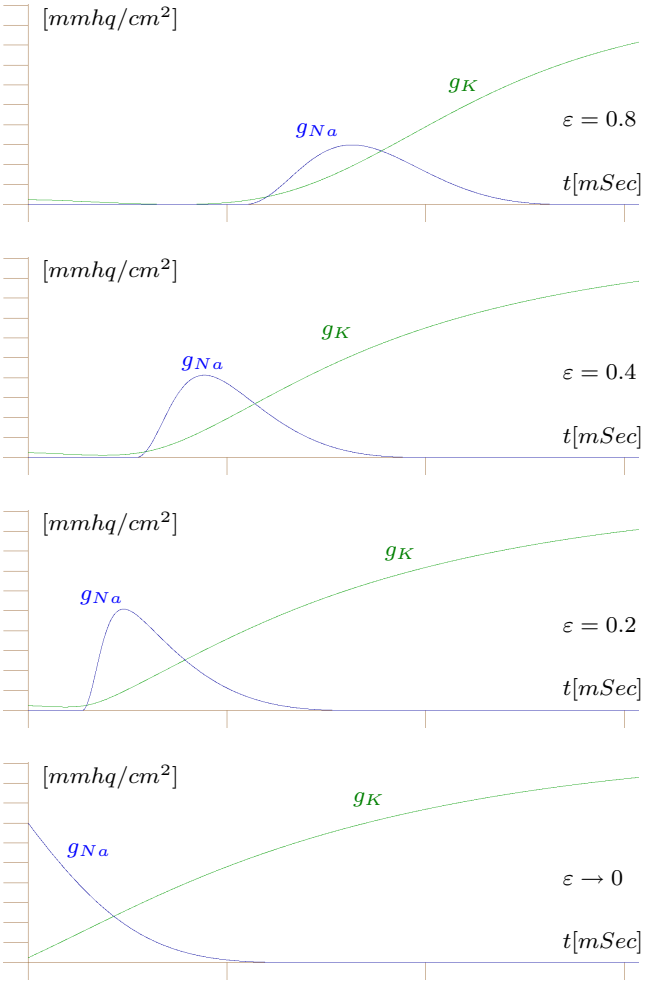

Fig. 12: Computed action potentials for the local nerve impulse example for different values of ε. The last picture shows a jump from F to G_1, see Fig. 11.

aforementioned constraint is eliminated, thereby allowing the system to return to the equilibrium point E of the original vector field.

As the trajectory from F to H is dominated by the fast component of the vector field in x direction, it is natural to consider instead a jump from F to G_1, followed by the trajectory of the modified slow vector field leading to H along M. Both paths are depicted in the figure in red resp. blue.

A plot of the resulting quantities g_{Na} and g_K along the computed trajectories are known as so-called action potentials and depicted in Figure 12. These results are consistent with the discussion of Woodcock, see in particular Figures 19 and 20 in [14] where a clamp voltage of 38mV has been used.

4.4 Electrical circuits

Parts of the presented framework have been applied in the context of studying examples taken from electrical engineering, see e.g. [11, 17, 19]. A main objective in this context is to determine stable operating points of electrical circuits. The conventional design cycle employs circuit simulators for this purpose, which unfortunately are known to fail for certain idealized circuits. Common methods to overcome this difficulty and to make the simulations converge depend on introducing parasitic inductances and capacitances into the circuit layout. While from a mathematical perspective the latter approach corresponds to the so-called Tikhonov regularization, it is unsatisfactory in practice, since it depends essentially on the experience of the designer and is prone to error. For more background related to these issues we refer to [18, 20].

Our approach allows to determine operating points of electrical circuits without using parasitic elements and the corresponding regularization techniques.

Figure 13 shows an example modeling an emitter-coupled multi-vibrator discussed in [17]. The governing equations are given by a DAE system of the form

$$f(u_{D_1}, u_{D_2}, u_C) = 0 \ , \quad g(u_{D_1}, u_{D_2}, u_C, \dot{u}_C) = 0 \ .$$

The specific expressions for f and g can be found in [17]. In this example the slow manifold M is the one-dimensional curve shown in gray, while jump and hit sets are zero-dimensional, consisting of isolated points on M. The jump space is spanned by the u_{D_1} and u_{D_2} directions.

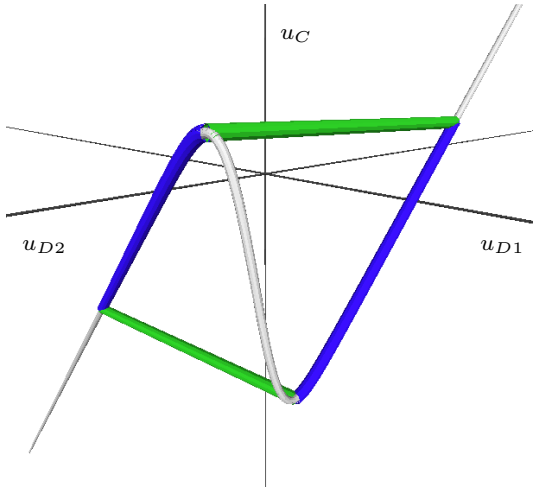

Fig. 13: Closed limit cycle of a multi-vibrator with one capacitance. The state manifold, the trajectory of the slow vector field and the jumps are indicated in gray, blue and green, respectively.

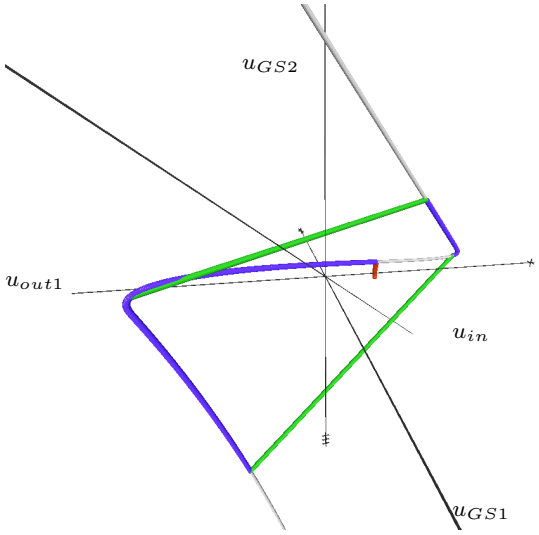

Fig. 14: Visualization of the MOS flip flop model described in [19] with colors as in Fig. 13. Additionally, the homotopy path leading to an initial point on M is shown in red.

As a second example we have considered a MOS flip flop model, see [19], which is characterized by a one-dimensional state manifold embedded in a four-dimensional space spanned by the parameters denoted as $u_{GS1}, u_{GS_2}, u_{in}, u_{out1}$. The jump space here is three-dimensional and spanned by the u_{GS1}, u_{GS2} and u_{out1} directions. The corresponding result is shown in Fig. 14.

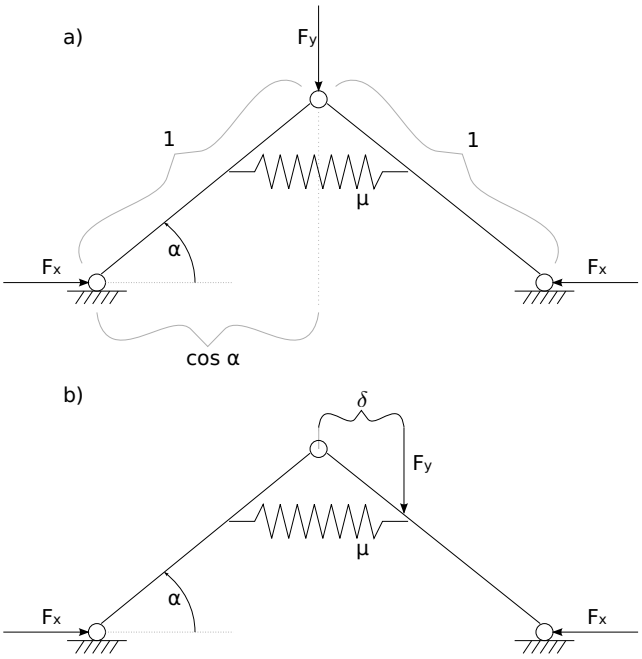

Fig. 15: a) The Euler arch. b) The extended Euler arch.

4.5 Euler arch

As an example for a mechanical system we consider the so-called Euler Arch adapted from [26]. It consists of two rigid arms being connected by a spring of stiffness μ that tends to keep them at 180 degrees. There is one force F_x compressing the two arms and another force F_y acting from the top. The position of the arms can be described using an angle parameter α as shown in Fig. 15a. Increasing the force F_x makes the construction buckle upwards, while increasing F_y leads to the so-called catastrophe in which it suddenly snaps into a state buckling downwards. As discussed in [26], the set of valid states (F_x, F_y, α) is a two-dimensional manifold described by the equation

$$4\mu\alpha + F_y \cos(\alpha) - 2F_x \sin(\alpha) = 0$$

We extend this example by modeling a feedback system in terms of a vector field, thereby equipping the manifold with a dynamic. If F_x is low, the feedback system will increase it. As F_x reaches a designated value, the variation of F_x slows down smoothly while F_y starts to increase. As F_y increases, the system finally reaches a situation as described above, where a sudden jump has to occur. We model this behavior using the following slow vector field

$$\dot{F}_x = \frac{1}{e^{2(F_x-3.25)}+1} \qquad \dot{F}_y = 10 - \frac{20}{e^{2(F_x-3.25)}+1} \,.$$

Figure 16 visualizes the results of the corresponding computations.

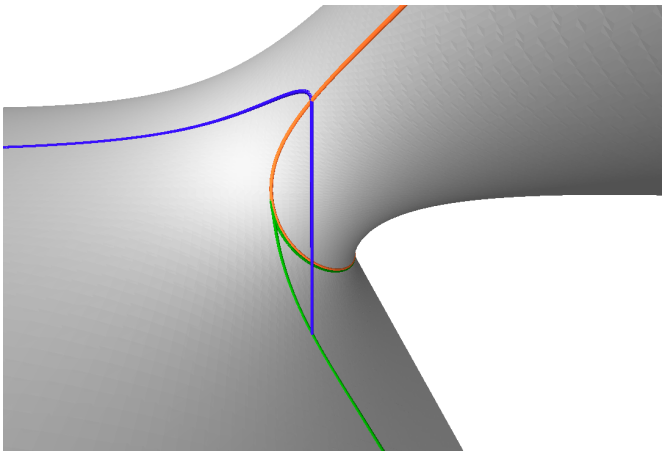

Fig. 16: Results of modeling the Euler arch based on the discussion in [26]. The blue path represents the trajectory of the given slow vector field incorporating a jump.

4.6 Extended Euler arch

In this final example we extend the model of the Euler arch described in the previous section by introducing a new degree of freedom δ that denotes the horizontal distance from the center to the position where F_y is applied. Thus F_y may act at a point differing from the center as shown in Fig. 15b.

By a derivation similar to [26] we arrive at the following equation implicitly characterizing the system's set of admissible states as a three-dimensional manifold embedded in four-dimensional Euclidean space whose axes are identified with the parameters α, F_x, F_y and δ:

$$(4\mu\alpha - 2F_x \sin(\alpha))\cos^2(\alpha) + F_y(\cos^3(\alpha) - \delta) = 0 \ .$$

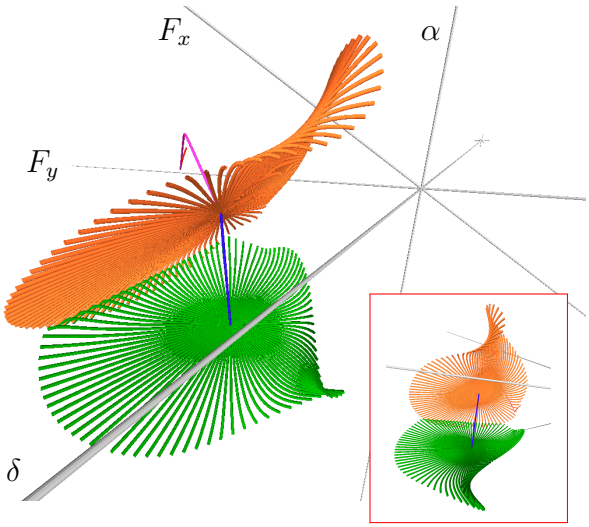

Fig. 17: Two-dimensional jump set (orange) and the corresponding hit set (green) of the state manifold for the extended Euler arch example.

By applying our computational methods, we could successfully determine initial points on the manifold and on the jump set α, resp. on the hit set β. Note that the latter sets are two-dimensional in this example. Thus, as discussed in Sec. 3.5, we have relied upon geodesic polar coordinates to parametrize α while tracing the corresponding projections on β in parallel. The result of this approach is illustrated in Fig. 17, showing a projection of the four-dimensional space.

5 Conclusion and Outlook

In this work we have discussed how a toolkit of geometrically inspired methods can be used to analyze a variety of dynamical systems governed by so-called slow-fast vector fields and corresponding systems of differential algebraic equations.

Our approach consists in explicitly computing so-called jump and hit sets on the slow manifold M, allowing us to capture the dynamics of the corresponding model by tracing the slow component of the vector field along M while incorporating jumps in direction of the fast component.

Note that while the state manifolds depicted in our examples require a sampling for visualization, our presented methods do not depend on them. They rely only upon a comparatively localized evaluation of the equations describing the given DAE system. In fact the particular representation of the underlying functions describing our DAE system does not matter. Therefore the presented approach scales efficiently to higher dimensions as realized in our framework.

As the considered equations are in general nonlinear, our approach incorporates extended homotopy methods to determine initial points and exploits numerical continuation techniques as well as geodesic polar coordinates to obtain explicit parametrizations. Our methods are numerically stable and improve upon classical approaches which trace the slow-fast vector field directly and therefore suffer from the large gap between the involved scales.

In the future we plan to further optimize our approach involving geodesic polar coordinates by taking into account the non-injectivities induced by them. Within this discussion concepts such as the cut-locus and focal sets have to be considered, see [23, 16].

Moreover we plan to address questions related to the existence of multiple connected components of the state manifold. In this context, geodesic polar coordinates

are also particularly suitable. More precisely, any two points lying in the same connected component can be captured within the same GPC system. This remains a promising topic for future research.

References

1. A.L.Hodgkin, A.F.Huxley: A Quantitative Description of Membrane Current and its Application to Conduction and Excitation in Nerve. J.Physiol. **117**, 500–544 (1952)
2. A.L.Hodgkin, A.F.Huxley: Currents carried by Sodium and Potassium Ions through the Membrane of the Giant Axon of Loligo. J.Physiol. **116**, 449–472 (1952)
3. Allgower, E.L., Georg, K.: Introduction to Numerical Continuation Methods. Classics in applied mathematics. SIAM (2003)
4. do Carmo, M.P.: Riemannian Geometry. Birkhauser (1992)
5. F. Memoli, G. Sapiro and S. Osher: Solving variational problems and partial differential equations mapping into general target manifolds. Journal of Computational Physics pp. 263–292 (2004)
6. G.Golub, W.Kahan: Calculating the singular values and pseudo-inverse of a matrix. J. SIAM Numer. Anal. Ser.B **2** (1965)
7. Guckenheimer, J., Haiduc, R.: Canards at folded nodes. Mosc. Math. J. **5**(1), 91–103 (2005)
8. Guckenheimer, J., Hoffman, K., Weckesser, W.: Numerical Computation of Canards. International Journal of Bifurcation and Chaos **10**(12), 2669–2687 (2000)
9. Guckenheimer, J., Hoffman, K., Weckesser, W.: Global analysis of periodic orbits in the forced van der Pol equation. In: H.W. Broer, B. Krauskopf, G. Vegter (eds.) Global Analysis of Dynamical Systems – Festschrift dedicated to Floris Takens for his 60th birthday, pp. 261–276. IOP Press (2003)
10. Guillemin, V., Pollack, A.: Differential topology, vol. 370. American Mathematical Soc. (2010)
11. Mathis, W., Blanke, P., Gutschke, M., Wolter, F.-E..: Nonlinear Electric Circuit Analysis from a Differential Geometric Point of View. ITG-Fachbericht-ISTET 2009 pp. 30,167–30,167 (2009)
12. Nass, H.: Medial Axis on Riemannian Manifolds. Ph.D. thesis, Leibniz Universitaet Hannover (2007)
13. Patrikalakis, N.M.: Shape Interrogation for Computer Aided Design and Manufacturing. Springer (2002)
14. Steward, I., Woodcock, A.E.R.: On Zeeman's Equations for the Nerve Impulse. Bulletin of Mathematical Biology **43**, 279–325 (1981)
15. Tchizawa, K.: An Analysis of Nonlinear Systems with Respect to Jump. Yokohama mathematical Journal **32**, 203–214 (1984)
16. Thielhelm, H., Vais, A., Brandes, D., Wolter, F.-E..: Connecting geodesics on smooth surfaces. The Visual Computer (2012)
17. Thiessen, T., Gutschke, M., Blanke, P., Mathis, W., Wolter, F.-E..: Numerical analysis of relaxation oscillators based on a differential geometric approach. In: International Conference on Signals and Electronic Systems, pp. 209 –212 (2010)
18. Thiessen, T., Gutschke, M., Blanke, P., Mathis, W., Wolter, F.-E. .: A numerical approach for nonlinear dynamical circuits with jumps. In: European Conference on Circuit Theory and Design (2011)
19. Thiessen, T., Gutschke, M., Blanke, P., Mathis, W., Wolter, F.-E..: Differential Geometric Methods for Jump Effects in Nonlinear Circuits. In: 20th Edition of the Nonlinear Dynamics of Electronic Systems (2012)
20. Thiessen, T., Mathis: Geometric Dynamics of Nonlinear Circuits and Jump Effects. International Journal of Computations & Mathematics in Electrical & Electronic Engineering **30**(4), 1307–1318 (2011)
21. Thom, R.: Structural Stability and Morphogenesis. W. A. Benjamin, inc. Advanced Book Program (1975)
22. Wolter, F.-E..: Distance function and cut loci on a complete riemannian manifold. Arch. Math. **1**(32), 92–96 (1979)
23. Wolter, F.-E.: Cut Loci in Bordered and Unbordered Riemannian Manifolds. Ph.D. thesis, TU Berlin (1985)
24. Wolter, F.-E.., Tuohy, S.T.: Approximation of high-degree and procedural curves. Engineering with Computers **8**(2), 61–80 (1992)
25. Zangwill, W.I., Garcia, C.B.: Pathways to solutions, fixed points, and equilibria. Prentice-Hall, Englewood Cliffs, NJ (1981)
26. Zeeman, E.C.: Catastrophe theory: selected papers, 1972-1977. Addison-Wesley (2000)